CHAPTER 6

Development of Polyurethane Composite Films using Castor oil

6.1. Introduction

Bacteria can be found on a wide range of surfaces, with a concentration particularly high at solid-liquid interfaces. Bacteria also have the capability to create biofilms, wherein bacterial colonies are tightly packed and caged within an extracellular polymeric matrix. A simple way to remove bacterial biofilms from surfaces or interfaces requires to develop of self-disinfecting properties.[1] Various metal and metal oxide nanoparticles are also applied as coatings on the infected surfaces to hinder the growth of harmful organisms.[2,3] In the past few years, many antimicrobial polymeric materials have been synthesized using variety of materials like metal nanoparticles (Ag and Cu), metal oxides (ZnO, TiO_2, CuO), organic acids (benzoic acid, sorbates), enzymes (glucose oxidase, lysozyme), naturally active compounds (curcumin, essential oil, pomegranate-rind extract, and various biopolymers), triclosan, antibiotics, and other functional ingredients to eliminate the harmful microbes.[4,5] Many researchers have also prepared polymeric composite materials that have both antimicrobial and antioxidant properties, in which polyurethane-based composites are incredibly adaptable materials.[6]

Polyurethanes (PUs) offers a wide range of applications in the form of adhesives, coating, and foams.[7] The antimicrobial activity of PU polymeric materials is an important property used in food and other packaging products, as normally PU materials could easily be colonized through microbes that may also lead to health-related issues in humans.[8–10] Incorporating metal nanoparticles and bioactive components into the synthesis of PU based composite is one of the main aims of the researchers to improve the antimicrobial properties of PU. Hence, it is always necessary to improve the antimicrobial activities of PU polymers for their better food and packaging applications in addition to enhancing their electrical, mechanical, and thermal properties. To overcome this issues, PU-based composite materials have been developed using various nanofillers like ZnO,[11] Au,[12] AgNPs,[13] SiO_2NPs,[14] GNPs,[15] and CNTs[16] on the matrices of PU polymers.[17,18] Among various nanofillers, SiO_2NPs act as an ideal reinforcing agent or nanofiller for the synthesis of versatile PU-based nanocomposite due to their unique structure, high surface area, excellent thermal stability, and better mechanical strength.[19,20] Not only that, the incorporation of SiO_2NPs into the PU matrix enhances the performance of polymers and imparts some novel properties to the PU matrix.[21,22]

Most of the PUs are synthesized with the larger usages of petrochemical polyols and hazardous isocyanates, which are non-renewable resources.[23,24] As a result, many researchers

have made substantial efforts to develop bio-based PUs, which can be prepared by using polyols from natural sources.[25] Several researchers have employed PU prepared from natural components or oils to fabricate antibacterial bio-based PU composites.[26]

Nowadays, bio-based PU composites have received much attention as multifunctional materials that can be applied in various applications, such as thermoset, foam, coating, thermoplastic elastomers, adhesives, and medical fields.[19,27] The advantages of bio-based PU composite materials are low cost, better strength, good thermal properties, and especially biocompatibility and biodegradability.[27] The most dominant biosource of polyol to synthesize biocompatible PUs is castor oil (CO), due to its non-edible nature and distinctive hydroxyl group structure.[28,29] There were not many studies attempted by researchers to incorporate natural antibacterial bioactive compounds such as curcumin in the biobased PU composites and therefore, researchers have increasingly turned their attention to developing antibacterial PU by incorporating curcumin as a key ingredient due to its potent antimicrobial properties. Curcumin has ability to disorder bacterial cell membranes and inhibit cell growth.[30] When integrated into the PU matrix, curcumin not only imparts strong antibacterial activity but also enhances the biocompatibility of the material. The effectiveness of curcumin-incorporate PUs depends on the homogeneity and concentration of curcumin within the polymer matrix, ensuring the better expose on bacterial cells.[31] This innovative approach offers a safer and more sustainable solution for various applications, leveraging the antibacterial properties of bio-based PU composites.

To understand the importance of bio-based PU composite materials in food and packaging applications where composite materials should be stable structurally, thermally, and have potent antibacterial activity, we synthesized curcumin-incorporated CO-based PU and PUS composite films using castor oil as a polyol for PU synthesis, curcumin as an antibacterial agent, and silica nanoparticles (SiO_2NPs) as nanofiller. The SiO_2NPs were extracted from rice husk (RH). The swell-encapsulation-shrink technique has been used to incorporate the curcumin into the PU and PUS composite films. The degree of swelling, leaching behavior, structure (ATR-FTIR), surface morphology, chemical composition, optical properties, photoluminescence, thermal properties, wettability, and antibacterial activity of all the synthesized composite films were studied for their further potent applications in food and packaging materials.

6.2. Experimental

6.2.1. Materials

Methyl ethyl ketone (MEK), ethanol, and curcumin were purchased from Loba Chemie (Mumbai, India). Isophorone diisocyanate (IPDI) was obtained from Merck Limited (Germany). Dibutyltin dilaurate was procured from TCI (India). Rice husk was sourced from the local market.

6.2.2. Methods

6.2.2.1. Synthesis of SiO_2NP using rice husk

SiO_2NPs were synthesized from rice husk ashes using a chemical technique involving acid pre-treatment, as shown in **Figure 6.1**. Initially, rice husks were burned to collect its ashes (RHA). 3 gm of RHA was taken into a beaker and 45 mL of 10% HCl were gradually added. The acidic RHA solution was stirred for 2 hrs to remove metal ions. These metal-ion-depleted ashes, referred as leached RHA (LRHA), were then filtered, washed with deionized water, and dried in a vacuum oven at 80°C for 48 hrs. The resultant dry powder was calcinated in a muffle furnace at atmospheric pressure for 2 hrs at 700°C, resulted the white SiO_2NP powder.

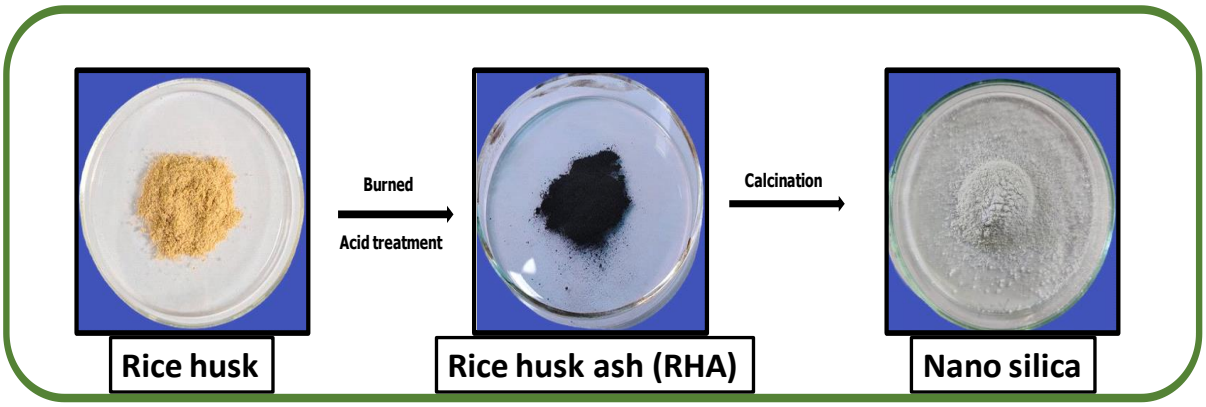

Figure 6.1. Synthetic route of SiO_2NPs from RHA

6.2.2.2. Preparation of CO-based PU and PUS composite films

The synthesis of CO-based PU and PUS composites was conducted in two steps, as shown in **Figure 6.2**. In the first step, the molar ratio of CO to IPDI was set at 1:2 (OH : NCO). Initially, CO was dried in a vacuum oven at 80°C overnight. The synthesis of PU polymer was carried out in a 3-necked 100 mL RBF arranged with a mechanical stirrer, thermometer, and N_2 gas inlet. When the temperature in the flask reached 60°C, CO was added with stirring at 160–200 RPM and subsequently IPDI was added drop by drop under an N_2 atmosphere. The reaction was maintained at 60°±5°C for 2 hrs with DBTDL(catalyst) and

MEK(solvent). After the completion of CO-based PU formation, SiO_2NPs as nanofillers was added under sonication for 2 hrs, and then obtained CO-based PUS film which further casted at RT.

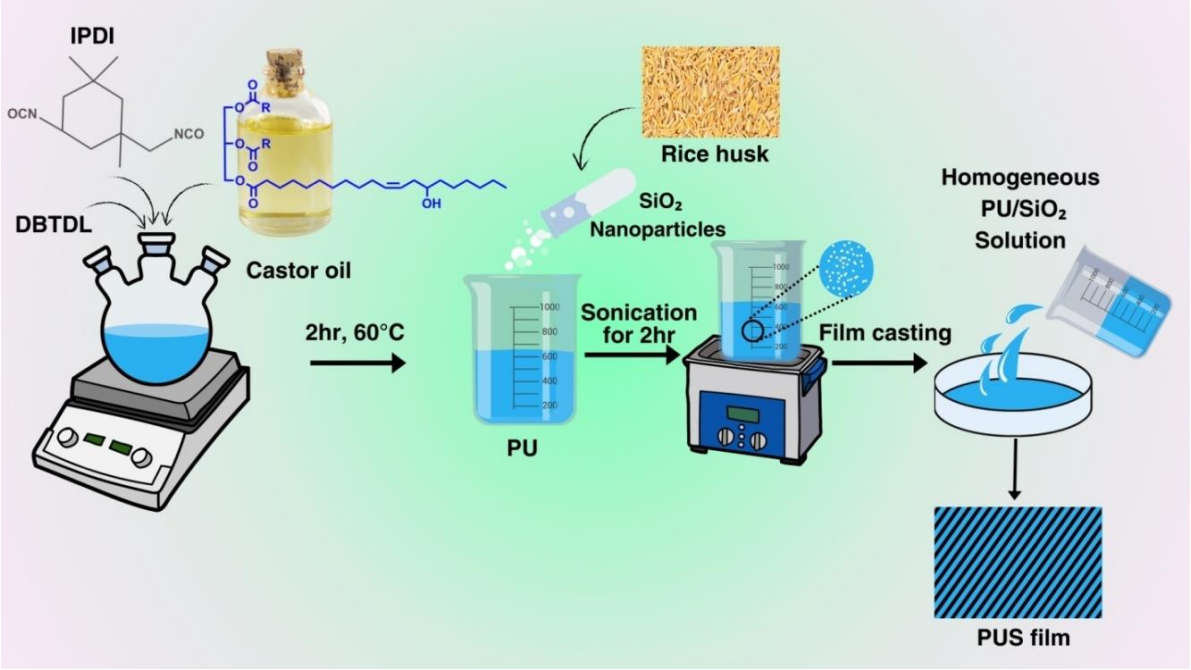

Figure 6.2. Synthesis of CO-based PU and PUS composite films

6.2.2.3 Preparation of Curcumin-incorporated CO-based PUC and PUSC composite films

The transparent CO-based PU and PUS composite films were submerged for 2 hrs in the 100 mL beaker containing the curcumin solutions (1.34 mg/mL curcumin dissolved in an ethanol). After that the developed CO-based PUC and PUSC composite films were properly dried in an oven at 60 °C for 24 hrs. **Figure 6.3** illustrates the procedure for developing CO-based PUC and PUSC composite films.

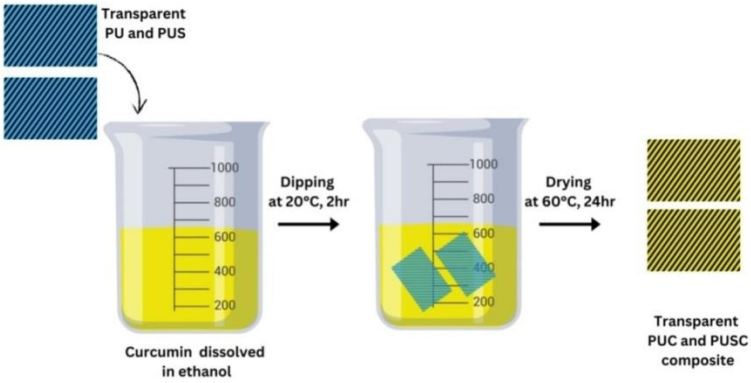

Figure 6.3. Development of CO-based PUC and PUSC composite films

6.2.3. Characterization of SiO_2NPs and CO-based PU and its composite films

6.2.3.1. ATR-FTIR

The ATR FTIR spectra of the SiO_2NPs, PU, PUS, PUC, and PUSC composite films were measured at ambient temperature in the air on a Bruker Tensor 11. The spectra were recorded with a spectral resolution of 4 cm^{-1} in the range from 500 to 4000 cm^{-1}.

6.2.3.2. DLS

The DLS analysis was used to determine the particle sizes in the form of average hydrodynamic dimeter (Dh) of the nanosilica at 28±0.5 °C using the Zetasizer Nano-ZSP system (Malvern, UK), which was outfitted with Nano ZS® software.

6.2.3.3. XRD

The SiO_2NPs are characterized by using XRD (Bruker, Model: D2 phaser, Germany).

6.2.3.4. EDX

EDX spectroscopy is used to find out each element present in the synthesized SiO_2NPs sample. Here, EDX samples was performed through a FE/SEM (Carl Zeiss Supra-55, Germany).

6.2.3.5. Swelling and leaching behavior of CO-based PU and its composite films

The swelling measurements of the CO-based PU, PUS, PUC, and PUSC composite films were carried out in toluene media at RT. Sample (1 x1 cm^2) pieces of composite film samples were dipped in the toluene solvent for 48 hrs. After removing excess solvent, each film sample was weighed. The swelling experiments were conducted in triplicate for each sample. The degree of swelling was determined using the gravimetric approach.[32]

$$\text{Degree of swelling} = \frac{(N - M_0)}{M_0}$$

Where, N and M_0 are the composite film weights after and before swelling, respectively.

The leaching behaviour of CO-based PUC and PUSC composite films was determined to immerse the film sample (1x1 cm^2) in 20 mL of distilled water for 24 hrs. UV-Vis spectra of an aliquot of water in which composite films were dipped were measured using a UV-Vis spectrophotometer (Perkin Elmer, Lambda 25). The spectra of water were taken before and after the immersion of the film (diluted with ethanol) to check the curcumin leaching. The experiments were done in triplicate.

6.2.3.6. AFM measurements of CO-based PU and its composite films

Surface morphology of PU, PUS, PUC, and PUSC composite films was characterized by atomic force microscopy (AFM, Nanosurf-3000, Switzerland). The measurements were conducted in tapping mode using a Tap190Al-G type cantilever with a silicon tip. The tip was coated with a 30 nm fine layer of aluminium on the detector side to enhance reflectivity. The cantilever had a resonance frequency of 190 kHz and a force constant of 48 Nm^{-1}. The Gwyddion software was used for image processing and determination of the root-mean-square (RMS) roughness for all the film samples.

6.2.3.7. XPS

AXIS Supra K-Alpha XPS equipment was used to record the XPS spectra of the PU, PUS, PUC, and PUSC composites using a monochromatic Al Kα – 1486.6 eV X-ray source. The sample size was taken 5 mm^2 for the measurement.

6.2.3.8. Optical analysis

The UV-Vis light barrier properties of CO-based PU and its composite films were measured by using UV-Vis spectrophotometer. The film samples were cut into proper rectangular pieces and well placed into the cuvette of spectrometer.

The photoluminescence measurements of the PUC and PUSC composites were carried out using an RF-6000 (Shimadzu, Japan) spectrofluorophotometer with an excitation wavelength range of 360 to 520 nm.

6.2.3.9. Wettability of CO-based PU and its composite films

"The wettability of the PU and its composite films has been checked using the contact angle measurements. The contact angle measurements were conducted by the Surface energy evolution system and result were analyzed by SEE system software. As a control the liquid we used deionized water. The relationship between contact angle and surface energy can be described by Young–Dupres equation:

$$(1 + \mathrm{COS}\theta)\gamma_{\mathrm{L}} = \mathrm{W_A}$$

Where, W_A is the surface energy and γ_L is surface tension of the liquid**"**

6.2.3.10. Thermal behavior of CO-based PU and its composite films

The Tg of the PU composite films was analysed using DSC measurements conducted with TA Instruments (DSC 200 F3 Maia, NETZSCH-India). The experiment were done in two cycles, in which the first cycle initiated from RT to 50°C, while the second cycle was performed in a temperature range of 50°C to 100°C with a constant heating rate of 10°C /min under a dry N_2 atmosphere. The TG analyzer (TA instrument STA 449 F3 Jupiter) was used

to find the weight loss of the film under an air atmosphere. The composite film was scanned from 25°C to 700°C at a heating rate of 10°C/min.

6.2.3.11. Antibacterial Activity of CO-based PU and its composite films

The antibacterial activity of the PU, PUS, PUC, and PUSC composite films was tested against bacterias. Antibacterial activities were performed by the standard ISO 22196 method using the *E.coli* and as gram-negative and *S.aureus* as gram-positive as the testing strains. The bacterial growth (R) reduction on the fabric sample was calculated as:

$$\% \, R = \frac{(N - M)}{N} \times 100$$

Where, R= Reduction rate of bacterial growth, N= Initial number of bacterial colonies and M= Number of bacterial colonies on coated fabrics after contact for 24 hrs.

6.3. Results and discussion

6.3.1. Characterization of SiO_2NPs

6.3.1.1. ATR-FTIR

Figure 6.4 shows the IR of SiO_2NP which was examined by ATR-FTIR in the range of 4,000–500 cm^{-1}. The strong band at 1,095 cm^{-1} corresponds to the asymmetric vibration of the siloxane bond (Si–O–Si). This bond forms the main backbone of the SiO_2 matrix. The absorption band at 801 cm^{-1} is assigned to the stretching vibration of Si–O–Si bond. The presence of a band at 962 cm^{-1} indicates the Si–O stretching vibration of the silanol group.

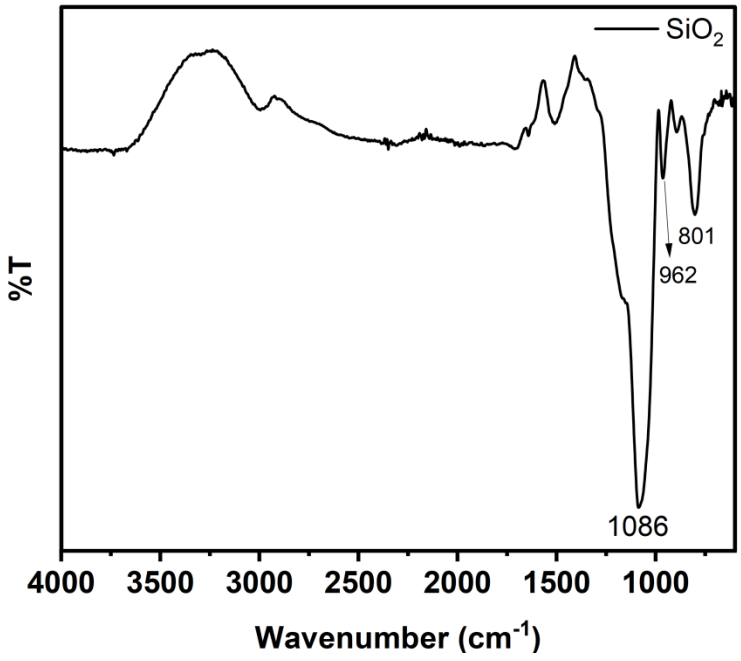

Figure 6.4. ATR-FTIR of SiO_2NPs synthesized using RHA

6.3.1.2 DLS of SiO_2NPs

The size of synthesized SiO_2NP is determined using DLS method. From the experimental results, it was observed that a single peak in **Figure 6.5** indicates the particles are of same size and the average particle sizes are 54.2 nm.

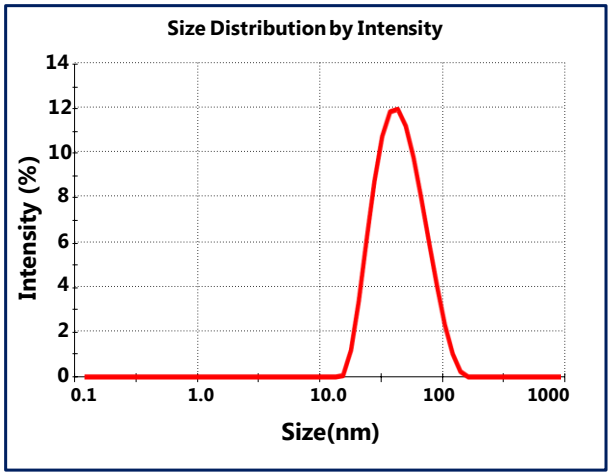

Figure 6.5. DLS of SiO_2NPs synthesized using RHA

6.3.1.3. XRD

XRD analysis was employed to characterize the synthesized SiO_2NPs. The obtained XRD pattern for SiO_2NP obtained from RHA is shown in the **Figure 6.6**. The presence of a broad peak centered at 22.8° in the powder diffraction pattern indicates the formation of the amorphous phase of SiO_2NP. Additionally, the wide range of the FWHM observed in the XRD pattern suggests that the SiO_2NPs are of small size.

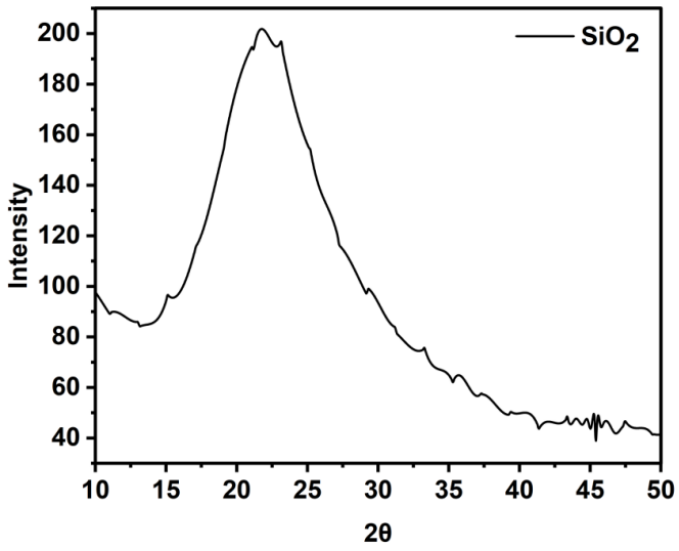

Figure 6.6. XRD pattern of SiO_2NPs synthesized using RHA

6.3.1.4. EDX

Figure 6.7 show that the presence of 45.87% w/w Si and 53.14% w/w O clearly indicates the formation of SiO_2NPs.

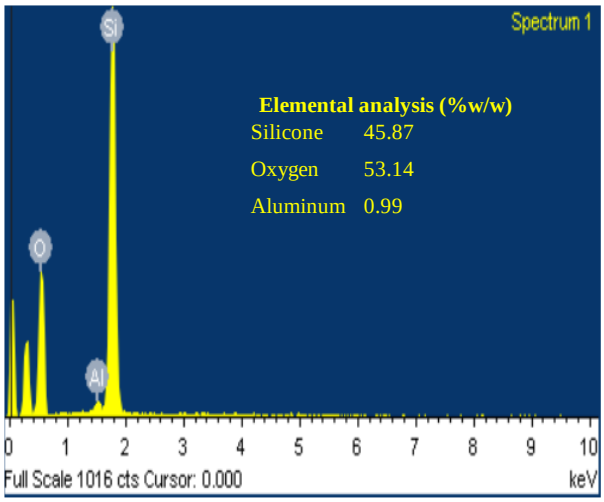

Figure 6.7. EDX spectrum of SiO_2NPs synthesized using RHA

6.3.2. Characterization of CO-based PU and its composite films

6.3.2.1 ATR FTIR

The ATR FTIR spectra of CO-based PU and PUS composite films were displayed in **Figure 6.8(a)**. The absorption peak of isocynate (-NCO) stretching at around 2250-2270 cm^{-1} was absent in the spectra of both PU and PUS, which clearly indicates the formation of urethane linkage. The stretching vibration peaks of N-H and C=O at 3335 and 1739 cm^{-1} also confirmed the formation of urethane linkage in PUs. All other characteristic peaks of PU, such as CH_3, CH_2, N-H, and C-O stretching, were also found at 2920, 2850, 1558, and 1234 cm^{-1}, respectively. The broad absorption peak at 1030 cm^{-1} of stretching vibration of the Si-O-Si group in the IR spectrum of PUS clearly proved the insertion of SiO_2NPs in the PU matrix. **Figure 6.8(b)** shows the ATR FTIR spectra of curcumin, PUC, and PUSC composite films. In Figure 4(b), curcumin showed a distinct absorption peak at 3506 cm^{-1} associated with phenolic OH stretching vibration. The peaks at 1628 cm^{-1} and 1508 cm^{-1} are stretching from carbonyl groups, whereas the peak at 1601 cm^{-1} belongs to aromatic C=C symmetric ring stretching. The peaks observed at 1275 cm^{-1} were a result of the C-O bond present in the enol. The peak at 1113 cm^{-1} stretching vibration from O-CH_3.[33] In the spectra of PUC and PUSC, the absorption peak at 1628 cm^{-1} attributed to the stretching vibration of the C=O groups. The stretching vibration peaks of aromatic C=C found at 1607 cm^{-1} and 1508 cm^{-1} were characteristic of the curcumin structure.[34] The presence of absorption peaks carbonyl

(C=O group) and aromatic (C=C symmetric ring) in both PUC and PUSC proved the incorporation of curcumin in the PU and PUS composite films.

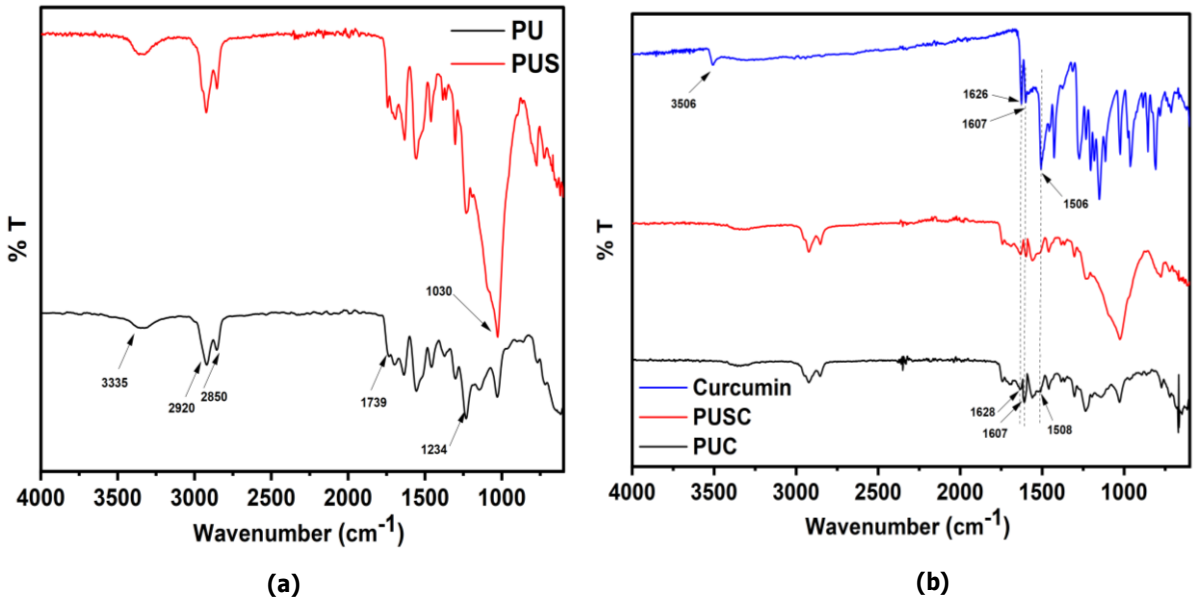

Figure 6.8. ATR FT-IR of (a) CO-based PU and PUS films (b) Curcumin, PUC, and PUSC composite films

6.3.2.2. Swelling and leaching behavior

Swelling behavior of the prepared PU, PUS, PUC, and PUSC composite films was observed in the toluene media. Swelling degree versus time for four different PU composite films is presented in **Figure 6.9 (a)**. The swelling degree of all PU film samples increases with time and, after 2 hrs, reaches saturation. Results clearly indicated that the swelling degree of PUC films was lowest compared to PU and other composite films. The swelling degree of PU increases due to lower crosslink density and higher interaction with the solvent, while incorporation of SiO_2NPs in PUS decreases the swelling degree. Here, the presence of SiO_2NPs in PU resulted in an increase in crosslink density, reduced free volume in the polymeric matrix, and restricted the interaction of solvent. It was found that the incorporation of curcumin in the PU shows the increase in swelling degree of PUC. Hence, when curcumin is added to the PU, its aromatic structure and platicizing effect enhance the interaction with toluene, leading to an increased swelling degree of the PUC. Here, PU and PUSC show an almost similar swelling degree, which indicates that, the development of composite film using SiO_2NPs and curcumin (PUSC) is gaining the same behavior in the organic medium. The swelling studies clearly confirmed the stability of composite films in common organic media, which benefits their application as packaging materials.

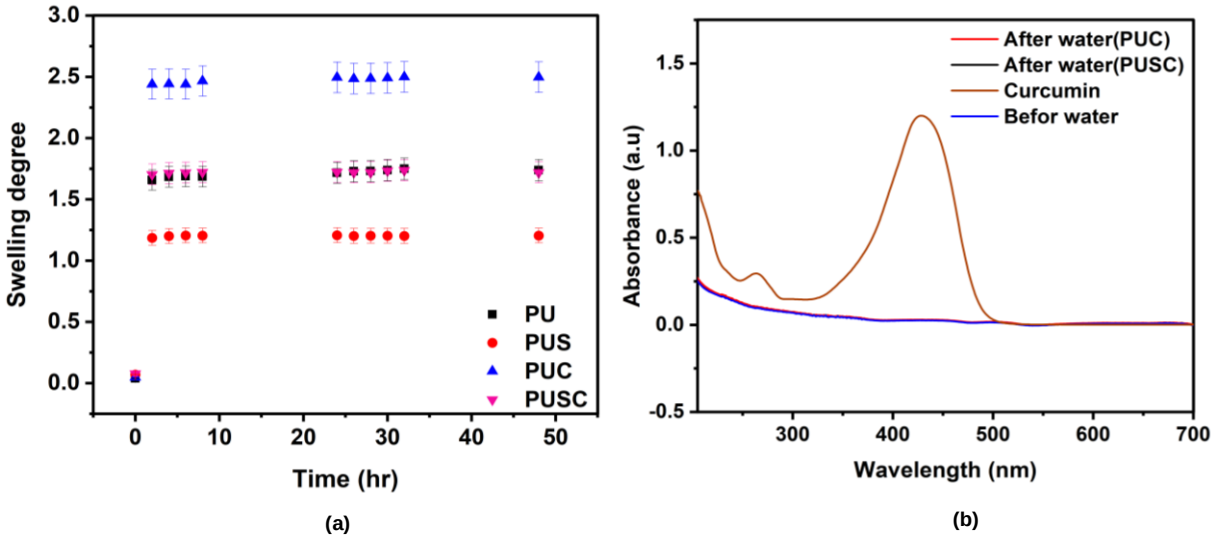

Figure 6.9. (a) Swelling degree synthesized CO-based PU and its composite films and (b) leaching behavior of CO-based PUC and PUSC composites films

UV-Vis spectroscopy was used to assess any possible curcumin leaching from the CO-based PU polymer matrix. The PUC and PUSC composite films were immersed in pure water separately for 24 hrs and after that the absorbance spectra of that water samples were recorded and shown in **Figure 6.9 (b)**. The absorbance spectrum of curcumin in ethanol was also included to observe any presence of curcumin in water after 24 hrs immersion. It was clearly shown that both films did not show any changes before and after a 24 hrs immersion in water as not found any absorbance peaks of curcumin in their respective water samples. These findings indicate that there was no leaching of curcumin from the PU and PUS polymer matrix, allowing the material to be used in any liquid media or in contact with humans.

6.3.2.3 AFM measurements of CO-based PU and its composite films

Figure 6.10 presents the surface morphology of CO-based PU, PUS, PUC, and PUSC composite films recorded by AFM. Here, root mean square (RMS) values of PU and PUS were calculated through a surface of 2 × 2 μm^2 and found to be 4.88 nm and 10.38 nm, respectively. RMS values of PUC and PUSC composite films were 2.64 nm and 6.88 nm, respectively. Hence, it was clearly understood that the curcumin incorporated into the PU matrix decreases the roughness of the surface of PU and PUS.[35] Therefore, curcumin is incorporated uniformly and homogeneously in the polymer matrix without any kind of aggregation and showed smoother surfaces.

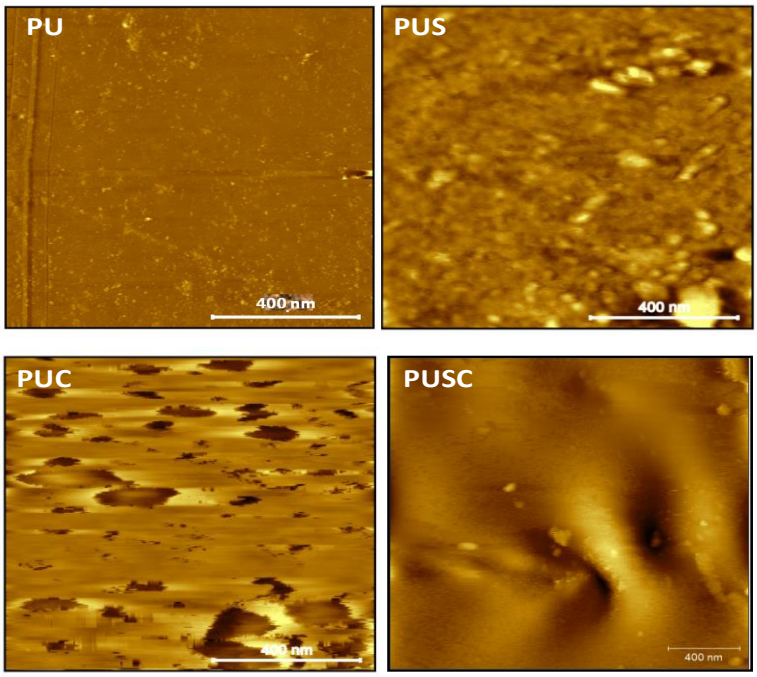

Figure 6.10. Top view AFM images of synthesized CO-based PU and its composite films

6.3.2.4. XPS analysis

The elemental analysis of CO-based PU and its composite films was performed through XPS spectroscopy, and results showed the presence of carbon (C), oxygen (O), and nitrogen (N) elements (shown in **Figure 6.11**).

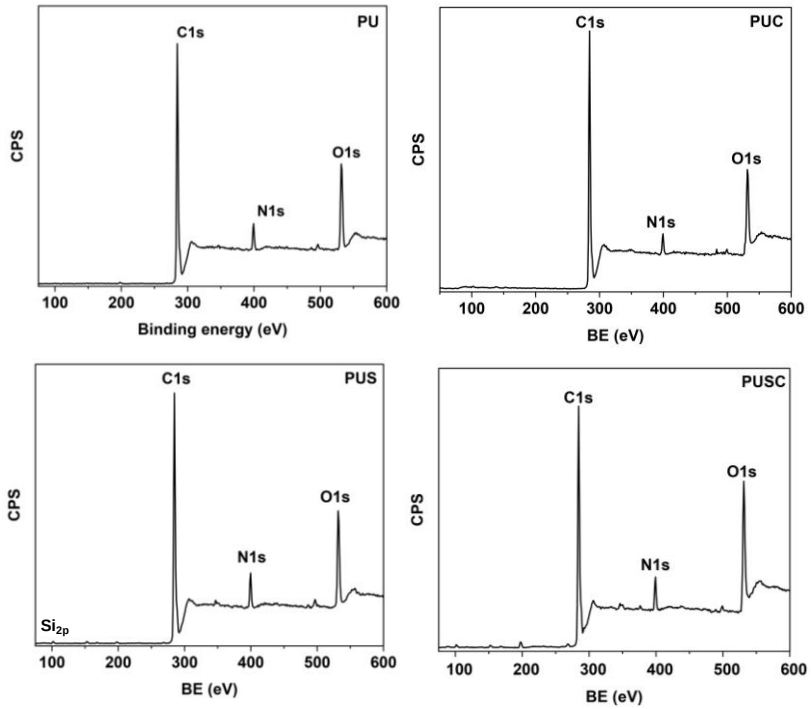

Figure 6.11. XPS survey spectra of PU and it's composite

The binding energy of the intensity peaks of these elements was used to determine the chemical composition of the PU and its composite films. The presence of C1s peak at nearby 284 eV in all the film samples is due to the presence of carbon atoms as the backbone of PU. The O1s peak at nearby 531 eV is because of the presence of oxygen atoms in ester linkage and phenolic group in the case of curcumin-based PU films in the all polymer films. The N1s peak at nearby 399 eV was confirming the presence of nitrogen atoms in the urethane linkages of the studied PU and its composite films. The Si2p peak at nearby 102 eV confirmed the presence of Si atoms in the studied PUS and PUSC composite films.

Figure 6.11 shows the fitted XPS spectra of C1s, O1s, and N1s peaks of CO-based PU, PUS, PUC, and PUSC composite films. Based on the data evaluated from XPS spectra, we interpretive the following: The oxygen content increases in PU to PUC (10.25→15.55 at %) and PUS to PUSC (9.34→14.04 at %) after the incorporation of curcumin in the composite films. The high resolution spectra of the C1s region in composite films showed many contributions to the peak envelope. Here, the assignments of the peaks were done based on PU film, which is derived from IPDI and CO. The assignments C1s spectra include C-C (284.61 eV and 284.53 eV), C-O (285.75 eV and 285.eV), C=O (286.88 eV and 286.57eV), NC=O (288.81 eV and 288.49 eV) and OC=O (289.63 eV and 289.46 eV) which confirms the urethane linkage. The O1s spectra of PU and PUC composites show three peaks at binding energies of 531.4, 532.7, and 533.6 eV and 531, 532.1, and 533.2 eV, respectively. These peaks can be assigned to three different types of oxygen-containing functional groups in the films: carbonyl (C=O), ether (C-O), and carboxylate (C-O*-C=O). The carbonyl peak is slightly shifted to lower binding energy (531 eV) in the PUC spectrum. Such a shift is found due to the electron-withdrawing effect of the curcumin molecules present in the composite. The ether peak is also slightly shifted to lower binding energy (532.1 eV) because of the hydrogen bonding between the ether groups and the curcumin molecules. The carboxylate peak is not significantly moved in the PUC spectrum.

The high-resolution spectra of CO-based PUS and PUSC (Shown in **Figure 6**) in the C1s region of the composite films showed multiple contributions to the peak envelope. The assigned C1s spectra include C-C (284.55 eV and 284.43 eV), C-O (285.43 eV and 285.40 eV), C=O (286.46 eV and 286.41 eV), NC=O (288.77 eV and 288.07 eV), and OC=O (289.66 eV and 288.93 eV). The O1s spectra of the PUS and PUSC composites display three peaks at binding energies corresponding to C=O (531.50 eV and 531.10 eV), C-O (532.95 eV and 531.67 eV), and C-O, -C=O (533.66 eV and 533.60 eV). XPS data clearly proved that the

curcumin incorporated in the CO-based PU films and enhanced the antibacterial properties in PU films for its further application.

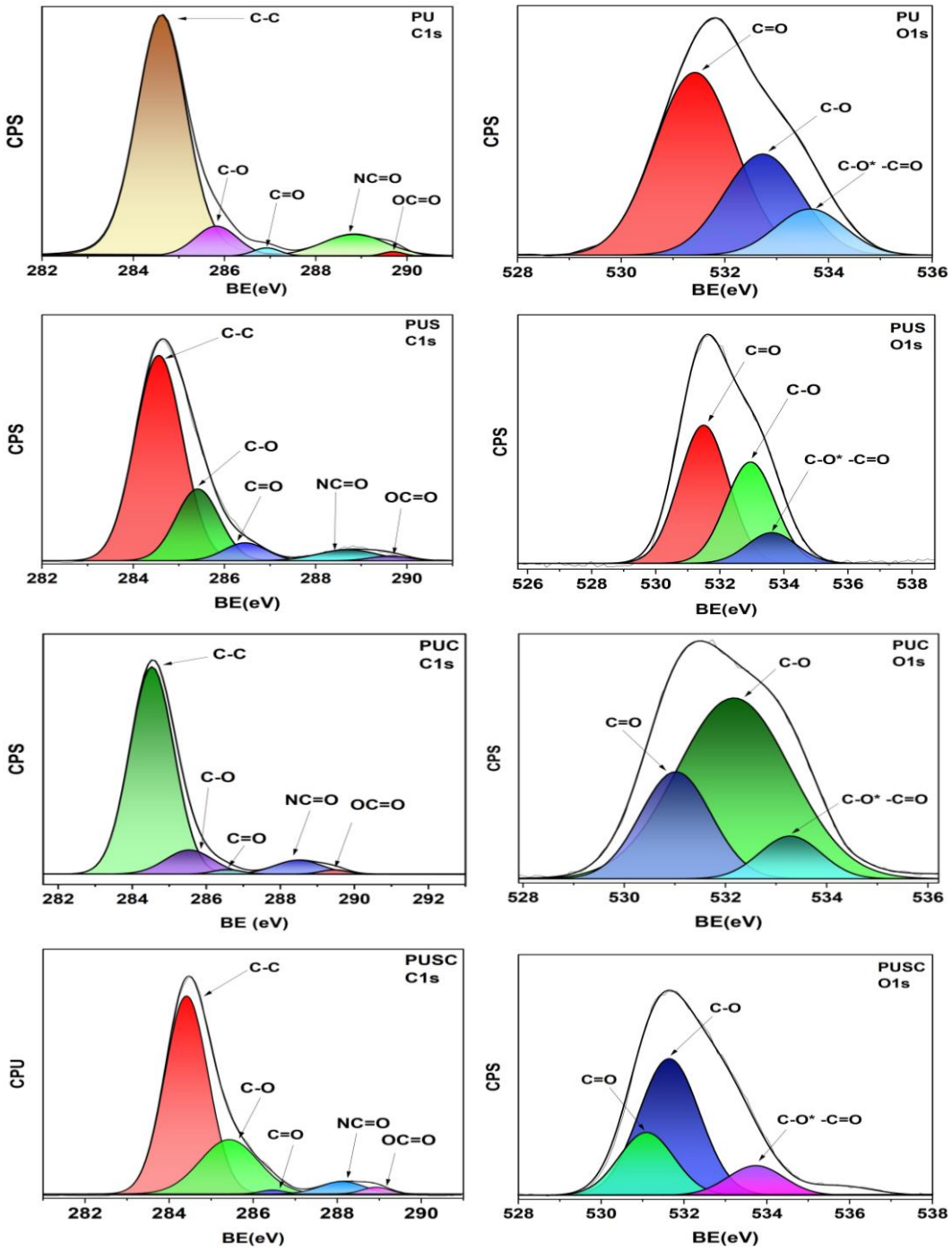

Figure 6.11. Fitted XPS spectra of synthesized CO-based PU and its composite films

6.3.2.5. Optical properties

In **Figure 6.12**, the UV-Vis spectra demonstrated greater absorbance signals for CO-based PUC and PUSC compared to PU and PUS composite films. The presence of curcumin in PUC and PUSC composite films confirmed through the characteristic absorption peak at

424 nm, which was absence in PU and PUS films. We also carried out PL studies on PUC and PUSC composite films. **Figure 6.13** shows the PUC and PUSC composites PL spectra at various excitation wavelengths. The maximum PL strength was observed at 526 nm for PUC and 528 nm for PUSC. For different excitation wavelengths (360-520 nm) there is a green emission centered between 525 and 530 nm.[35] The PL of curcumin-incorporated PU films is a phenomenon where the curcumin molecules incorporated within the film absorb photons and then emit green light.

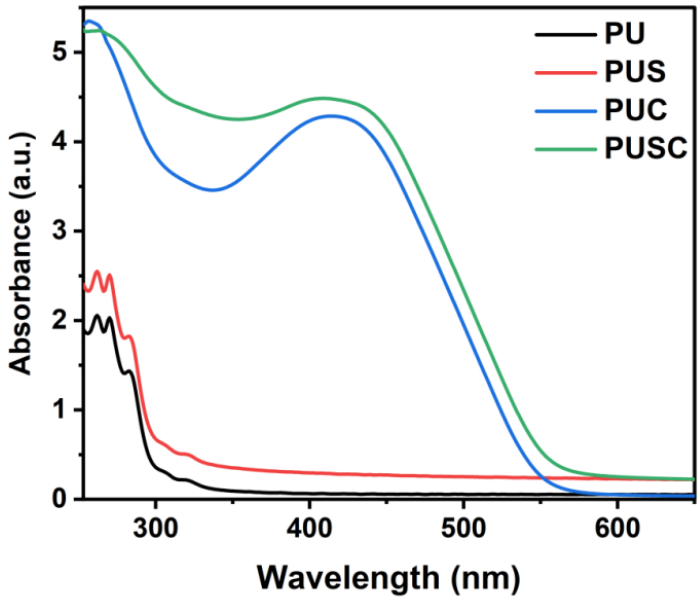

Figure 6.12. Optical Properties of synthesized CO-based PU and its composite films

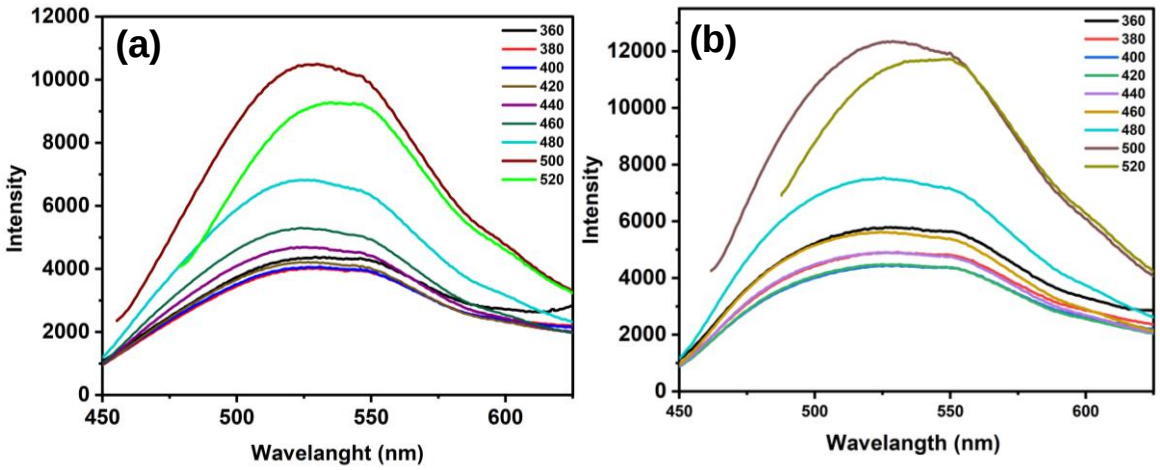

Figure 6.13 Photoluminescence of CO-based (a) PUC and (b) PUSC composite films

6.3.2.6. Wettability

To examine the wettability of CO-based PU, PUS, PUC, and PUSC composite films, contact angle experiments were performed by putting water droplets on the surfaces of PU films (shown in **Figure 6.14**). The contact angles were observed 78° for PU, 73° for PUS, 75° for PUC, and 68° for PUSC, respectively. The incorporation of curcumin into the PU matrix contributed to a decrease in hydrophobicity, as evidenced by the reduced contact angles for PUC and PUSC. Using the Young–Dupre model, the surface energies were calculated and found 87.9359 mJ/m² for PU, 94.0846 mJ/m² for PUS, 91.6420 mJ/m² for PUC, and 100.0713 mJ/m² for PUSC films. The incorporation of curcumin showed to increase the surface energy and decreases contact angle, indicating improved wettability. Such change in surface properties is attributed to the introduction of polar functional groups from curcumin such as hydroxyl and carbonyl groups into the PU matrix, which increase the overall surface energy and made PU more compatible with polar substances. Hence, the water droplets were spread more easily over the PU surfaces and decrease the contact angles. Additionally, the inclusion of SiO_2NPs in PUSC also increases the surface roughness. According to the Wenzel model, SiO_2NPs was done PUSC surface more hydrophilic and, therefore, enhance the wettability by further reducing the contact angle.

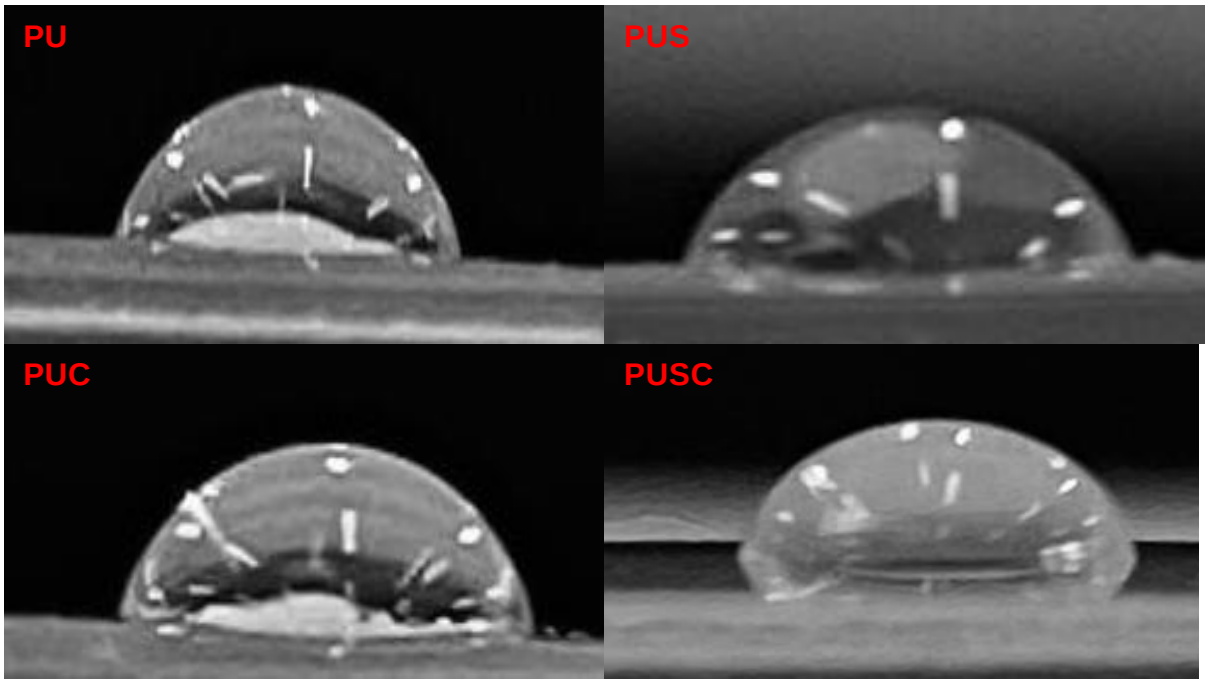

Figure 6.14. Contact angle picture of synthesized PU and its composite films

6.3.3. Thermal analysis

The DSC scan curve of CO-based PU and its composite films are shown in **Figure 6.15 (a)**, and the Tg of the composite films is given in **Table 6.1**. As observed in **Table 6.1**,

with the addition of SiO_2NPs and curcumin, the Tg for PU and composite films ranged from 54°C to 62°C. PU exhibited the lowest Tg value, while PUSC had the highest. Due to Properly dispersed nanoparticles increase the surface area for interaction between the polymer and the filler, enhancing interaction at the nanoscale and leading to a more significant effect on the PUs thermal properties, including an increase in Tg. Similarly, the incorporation of curcumin introduces additional interfaces within the PU matrix, which can hinder the mobility of the polymer chains and require more energy to reach the glass transition state, thereby increasing the Tg. Additionally, the DSC thermograms reveal that all the samples exhibit a single Tg, with the absence of melting and crystallization peaks. This suggests compatibility between the hard and soft segments of the material, indicating homogeneity and amorphous of the PUs.

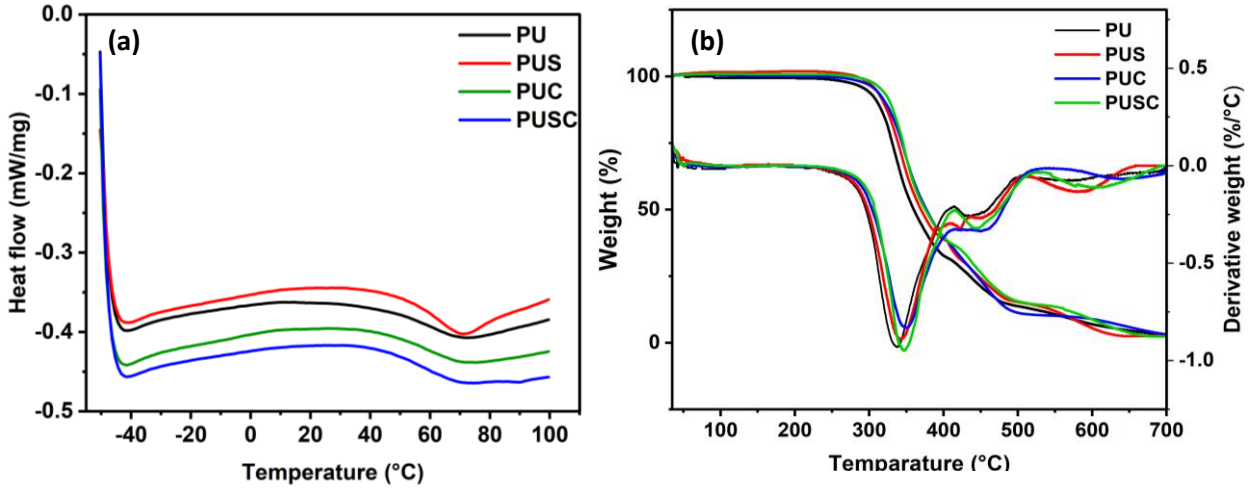

Figure 6.15. (a) DSC and (b) TAG/DTA thermograph of synthesized CO-based PU and its composite films

Table 6.1. Thermal analysis data of synthesized CO-based PU and its composite films.

Sample	Tg (°C)	$T_{initial}$(°C)	T_{10} (°C)	T_{50} (°C)	T_{95} (°C)	T_{Max} (°C)	Residue (%)
PU	54	230	309	359	618	337	2.94
PUS	60	263	318	369	570	342	2.31
PUC	56	258	320	375	648	349	3.17
PUSC	62	285	327	374	625	347	2.62

TGA and DTG thermograms, as shown in **Figure 6.15 (b)**, were used to represent the thermal characteristics of CO-based PU, PUS, PUC, and PUSC composite films. The thermal degradation of PUs occurred in three distinct stages, with the first stage being the most noticeable. Initially, urea and urethane bonds were broken, resulting in the formation of isocyanates, alcohols, 1° and 2° amines, olefins, and CO_2. The second stage shows the

decomposition of the hard segment of PU. The third stage displays the decomposition of the soft segment.[36] The DTG graphs in Figure 9 illustrate these three stages of PU breakdown upon heating. Notably, the DTG thermograms indicate that curcumin and SiO_2NPs enhance stability at high temperatures compared to the blank sample. The rapid weight loss observed during the first stage of degradation ranged from 230°C to 410°C, 263°C to 409°C, 258°C to 417°C, and 285°C to 416°C for PU, PUS, PUC, and PUSC, respectively. Subsequently, the second stage of degradation for each sample occurred between 410 and 495 °C, 409 and 504 °C, 417 and 522 °C, and 416 and 531 °C, respectively. Finally, the third stage of degradation was observed for PU, PUS, PUC, and PUSC at 495°C to 647°C, 504°C to 660°C, 522°C to 688°C, and 531°C to 693°C, respectively.

The thermal parameters, including the initial degradation temperature, T_{10}, T_{50}, T_{95} and the percentage of char residue remaining at 700°C, were obtained from the TGA and are shown in the **Table 6.1**. PUSC exhibits the highest thermal stability, with the highest initial decomposition temperature (285 °C) and a high midpoint decomposition temperature (374 °C), indicating it decomposes slower than the others. In contrast, PU has the lowest thermal stability, decomposing earlier (230 °C) and leaving less residue (2.94%). These results indicate that adding curcumin and silica enhances the thermal stability of polyurethane composites.

6.3.4. Antibacterial activity

Bacterial growth is a major cause of food adultration and wound health issues. Therefore, the antibacterial property is crucial for film materials used for food and packaging coating applications. Since *S. aureus* and *E. coli* are two common infectious bacterial species in the natural environment, the activities of CO-based PUC and PUSC composite films against these species were assessed in vitro. To test the suitability of the prepared curcumin-incorporated PU and PUS composite films (PUC and PUSC) for use as antibacterial composite films in food and packaging applications, the antibacterial activity was assessed using the contact killing bacteria experiment with gram-negative *E. coli* and gram-positive *S. aureus*. Curcumin may disrupt the integrity of bacterial cell membranes. Bacterial cell membranes are composed of lipids, and curcumin's inherent antibacterial nature allows it to interact with these lipids. This interaction can disrupt the structure and function of the cell membrane, leading to leakage of cellular contents, loss of vital nutrients, and ultimately cell death.[37,38] This mechanism is thought to be effective against both gram-positive and gram-negative bacteria, as both types of bacteria have cell membranes that can be targeted.[39] As shown in **Figure 6.16**, pure CO-based PU did not exhibit antibacterial activity against either

bacterium. Compared with the initial CFU (shown in **Table 6.2**), the synthesized composite films contain SiO_2NPs and/or curcumin displayed improved antibacterial properties against both types of bacteria. Antibacterial activity (%R) of PU, PUS, PUC, and PUSC composite films against *E. coli* was 45.48%, 86.46%, 99.89%, and 99.98%, respectively, and for *S. aureus*, it was 58.20%, 80.84%, 99.97%, and 99.99%, respectively. It can be concluded that the antibacterial properties increase with curcumin incorporation in PUC and PUSC films.

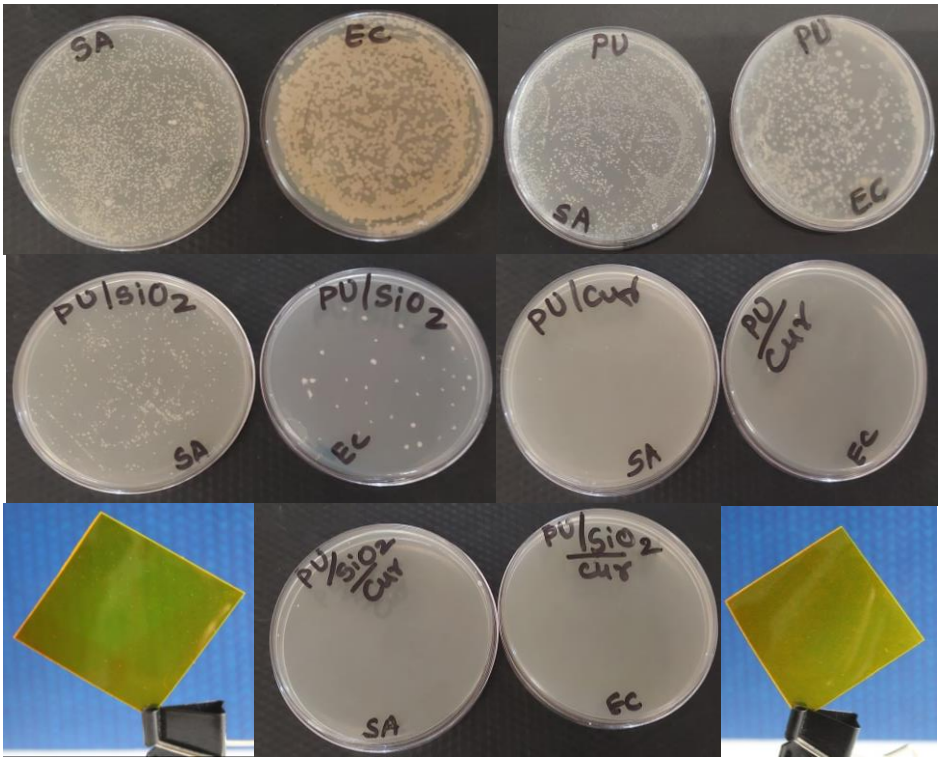

Figure 6.16. Antibacterial activity of the synthesized CO-based PU and its composite films and real images of synthesized PUC film (Left), PUSC film (Right)

Table 6.2. Antibacterial data synthesized CO-based PU and its composite films.

Sample	*E.coli* (CFU/cm^2)	%R	*S. aureus* (CFU/cm^2)	%R
Initial	2.66 x10^8	-	1.06 x10^9	-
PU	1.45 x 10^8	45.48	4.43 x 10^8	58.20
PUS	3.6 x 10^7	86.46	2.03 x 10^8	80.84
PUC	2.8 x 10^5	99.89	2.3 x 10^5	99.97
PUSC	1.6 x 10^5	99.93	1.1 x 10^5	99.99

All the results of different analyses proved that the CO-based PU films synthesized with the addition of SiO_2NPs as fillers and incorporation of curcumin as an antibacterial agent, here, PUSC composite film is superior amongst all, with a smoother surface and hydrophilicity, good compatibility, better thermal stability, and enhanced antibacterial activity.

6.4. References

(1) Kumar, L.; Bisen, M.; Harjai, K.; Chhibber, S.; Azizov, S.; Lalhlenmawia, H.; Kumar, D. Advances in nanotechnology for biofilm inhibition. *ACS Omega* **2023**, *8* (24), 21391–21409. https://doi.org/10.1021/acsomega.3c02239.

(2) Raghunath, A.; Perumal, E. Metal Oxide Nanoparticles as antimicrobial agents: a promise for the future. *International Journal of Antimicrobial Agent* ***2017***, *49* (2), 137–152. https://doi.org/10.1016/j.ijantimicag.2016.11.011.

(3) Taglietti, A.; Arciola, C. R.; D'Agostino, A.; Dacarro, G.; Montanaro, L.; Campoccia, D.; Cucca, L.; Vercellino, M.; Poggi, A.; Pallavicini, P.; Visai, L. antibiofilm activity of a monolayer of silver nanoparticles anchored to an amino-silanized glass surface. *Biomaterials* **2014**, *35* (6), 1779–1788. https://doi.org/10.1016/j.biomaterials. 2013.11.047.

(4) Wei, Q.; Wang, X.; Cheng, J.-H.; Zeng, G.; Sun, D.-W. Synthesis and antimicrobial activities of novel sorbic and benzoic acid amide derivatives. *Food Chemistry* **2018**, *268*, 220–232. https://doi.org/10.1016/j.foodchem.2018.06.071.

(5) Cetin-Karaca, H.; Newman, M. C. antimicrobial efficacy of plant phenolic compounds against *salmonella* and *escherichia coli*. *Food Bioscience* **2015**, *11*, 8–16. https://doi.org/10.1016/j.fbio.2015.03.002.

(6) Qiao, Y.; Duan, L. Curcumin-loaded polyvinyl butyral film with antibacterial activity. *e-Polymers* **2020**, *20* (1), 673–681. https://doi.org/10.1515/epoly-2020-0042.

(7) Akindoyo, J. O.; Beg, M. D. H.; Ghazali, S.; Islam, M. R.; Jeyaratnam, N.; Yuvaraj, A. R. Polyurethane types, synthesis and applications – a review. *RSC Advances* **2016**, *6* (115), 114453–114482. https://doi.org/10.1039/C6RA14525F.

(8) Abdo, S. M.; Youssef, A. M.; El-Liethy, M. A.; Ali, G. H. Preparation of simple biodegradable, nontoxic, and antimicrobial phb/pu/cuo bionanocomposites for safely use as bioplastic material packaging. *Biomass Conversion and Biorefinery* **2023**. https://doi.org/10.1007/s13399-022-03591-x.

(9) Mahanta, U.; Khandelwal, M.; Deshpande, A. S. Antimicrobial surfaces: a review of synthetic approaches, applicability and outlook. *Journal of Material Science* **2021**, *56* (32), 17915–17941. https://doi.org/10.1007/s10853-021-06404-0.

(10) Saleemi, M. A.; Lim, V. Overview of Antimicrobial polyurethane-based nanocomposite materials and associated signalling pathways. *European Polymer Journal* **2022**, *167*, 111087. https://doi.org/10.1016/j.eurpolymj.2022.111087.

(11) Zahra, M.; Ullah, H.; Javed, M.; Iqbal, S.; Ali, J.; Alrbyawi, H.; Samia; Alwadai, N.; Ibrahim Basha, B.; Waseem, A.; Sarfraz, S.; Amjad, A.; Awwad, N. S.; Ibrahium, H. A.; Somaily, H. H. Synthesis and characterization of polyurethane/zinc oxide nanocomposites with improved thermal and mechanical properties. *Inorganic Chemistry Communications* **2022**, *144*, 109916. https://doi.org/10.1016/j.inoche. 2022.109916.

(12) Habibzadeh, F.; Sadraei, S. M.; Mansoori, R.; Chauhan, N. P. S.; Sargazi, G. Nanomaterials supported by polymers for tissue engineering applications: a review. *Heliyon* **2022**, *8* (12). https://doi.org/10.1016/j.heliyon.2022.e12193.

(13) Li, S.; Zhang, Y.; Ma, X.; Qiu, S.; Chen, J.; Lu, G.; Jia, Z.; Zhu, J.; Yang, Q.; Chen, J.; Wei, Y. Antimicrobial lignin-based polyurethane/ag composite foams for improving wound healing. *Biomacromolecules* **2022**, *23* (4), 1622–1632. https://doi.org/ 10.1021/acs.biomac.1c01465.

(14) Hao, T.; Wang, Y.; Liu, Z.; Li, J.; Shan, L.; Wang, W.; Liu, J.; Tang, J. Emerging Applications of Silica Nanoparticles as Multifunctional Modifiers for High Performance Polyester Composites. *Nanomaterials* **2021**, *11* (11), 2810. https://doi.org/10.3390/ nano11112810.

(15) Fang, Z.; Huang, L.; Fu, J. Research status of graphene polyurethane composite coating. *Coatings* **2022**, *12* (2), 264. https://doi.org/10.3390/coatings12020264.

(16) Kausar, A. Self-healing polymer/carbon nanotube nanocomposite: a review. *Journal of Plastic Film & Sheeting* **021**, *37* (2), 160–181. https://doi.org/10.1177/ 8756087920960195.

(17) Farrokhi, Z.; Ayati, A.; Kanvisi, M.; Sillanpää, M. Recent advance in antibacterial activity of nanoparticles contained polyurethane. *Journal of Applied Polymer Science* **2019**, *136* (4), 46997. https://doi.org/10.1002/app.46997.

(18) Ahirwar, D.; Telang, A.; Purohit, R.; Namdev, A. A short review on polyurethane polymer composite. *Materials Today-Proceedings* **2022**, *62*, 3804–3810. https://doi.org/10.1016/j.matpr.2022.04.481.

(19) Wang, C.; Xu, F.; He, M.; Ding, L.; Li, S.; Wei, J. Castor oil-based polyurethane/silica nanocomposites: morphology, thermal and mechanical properties. *Polymer Composites* **2018**, *39* (S3), E1800–E1806. https://doi.org/10.1002/pc.24798.

(20) Kasi, G.; Gnanasekar, S.; Zhang, K.; Kang, E. T.; Xu, L. Q. Polyurethane-based composites with promising antibacterial properties. *Journal of Applied Polymer Science* **2022**, *139* (20), 52181. https://doi.org/10.1002/app.52181.

(21) Khdary, N. H.; Almuarqab, B. T.; El Enany, G. nanoparticle-embedded polymers and their applications: a review. *Membranes* **2023**, *13* (5), 537. https://doi.org/10.3390/membranes13050537.

(22) Mallakpour, S.; Naghdi, M. Polymer/SiO2 nanocomposites: production and applications. *Progress in Material Science* **2018**, *97*, 409–447. https://doi.org/10.1016/j.pmatsci.2018.04.002.

(23) Delavarde, A.; Savin, G.; Derkenne, P.; Boursier, M.; Morales-Cerrada, R.; Nottelet, B.; Pinaud, J.; Caillol, S. sustainable polyurethanes: toward new cutting-edge opportunities. *Progress in Polymer Science* **2024**, *151*, 101805. https://doi.org/10.1016/j.progpolymsci.2024.101805.

(24) Ganvit, V. M.; Sharma, R. K. recent developments of madhuca indica (mahua) oil-based polymers: a mini review. *Polymer from Renewable Resources* **2022**, *13* (1–2), 55–70. https://doi.org/10.1177/20412479221109909.

(25) Vijayan, J. G.; Chandrashekar, A.; AG, J.; Prabhu, T. N.; Kalappa, P. Polyurethane and its composites Derived from Bio-Sources: Synthesis, Characterization and Adsorption Studies. *Polymers and Polymer composites* **2022**, *30*, 09673911221110347. https://doi.org/10.1177/09673911221110347.

(26) Kaur, R.; Singh, P.; Tanwar, S.; Varshney, G.; Yadav, S. assessment of bio-based polyurethanes: perspective on applications and bio-degradation. *Macromol* **2022**, *2* (3), 284–314. https://doi.org/10.3390/macromol2030019.

(27) Rahman, I. A.; Padavettan, V. synthesis of silica nanoparticles by sol-gel: size-dependent properties, surface modification, and applications in silica-polymer nanocomposites—a review. *Journal of Nanomaterials* **2012**, *2012* (1), 132424. https://doi.org/10.1155/2012/132424.

(28) Chakraborty, I.; Chatterjee, K. polymers and composites derived from castor oil as sustainable Materials and Degradable Biomaterials: Current Status and Emerging Trends. *Biomacromolecules* **2020**, *21* (12), 4639–4662. https://doi.org/10.1021/acs.biomac.0c01291.

(29) Sardon, H.; Mecerreyes, D.; Basterretxea, A.; Avérous, L.; Jehanno, C. From Lab to market: current strategies for the production of biobased polyols. *ACS Sustainable Chemistry and Engineering* **2021**, *9* (32), 10664–10677. https://doi.org/10.1021/acssuschemeng.1c02361.

(30) Zheng, D.; Huang, C.; Huang, H.; Zhao, Y.; Khan, M. R. U.; Zhao, H.; Huang, L. Antibacterial mechanism of curcumin: a review. *Chemistry and Biodiversity* **2020**, *17* (8), e2000171. https://doi.org/10.1002/cbdv.202000171.

(31) Alven, S.; Nqoro, X.; Aderibigbe, B. A. Polymer-based materials loaded with curcumin for wound healing applications. *Polymers* **2020**, *12* (10), 2286. https://doi.org/10.3390/polym12102286.

(32) ganvit, v. m.; patel, v.; patel, m.; dharva, a.; sharma, r. k. synthesis, physicochemical and thermal properties of urethane-modified polyesteramide films using mahua and castor oil as sustainable resources. *Journal of Applied Polymer Science* **2024**, *141* (5), e54872. https://doi.org/10.1002/app.54872.

(33) M. Marković, Z.; P. Kepić, D.; M. Matijašević, D.; B. Pavlović, V.; P. Jovanović, S.; K. Stanković, N.; D. Milivojević, D.; Spitalsky, Z.; D. Holclajtner-Antunović, I.; V. Bajuk-Bogdanović, D.; P. Nikšić, M.; Marković, B. M. T. Ambient light induced antibacterial action of curcumin/graphene nanomesh hybrids. *RSC Advances* **2017**, *7* (57), 36081–36092. https://doi.org/10.1039/C7RA05027E.

(34) Oprea, S.; Potolinca, V. O.; Oprea, V. Synthesis and characterization of novel polyurethane elastomers that include curcumin with various cross-linked structures. *Journal of Polymer Research* **2020**, *27* (3), 60. https://doi.org/10.1007/s10965-020-036-6.

(35) Marković, Z.; Kováčová, M.; Mičušík, M.; Danko, M.; Švajdlenková, H.; Kleinová, A.; Humpolíček, P.; Lehocký, M.; Marković, B. T.; Špitalský, Z. Structural, mechanical, and antibacterial features of curcumin/polyurethane nanocomposites. *Journal of Applied Polymer Science* **2019**, *136* (13), 47283. https://doi.org/10.1002/app.47283.

(36) Carriço, C. S.; Fraga, T.; Carvalho, V. E.; Pasa, V. M. D. Polyurethane foams for thermal insulation uses produced from castor oil and crude glycerol biopolyols. *Molecules* **2017**, *22* (7), 1091. https://doi.org/10.3390/molecules22071091.

(37) Ratrey, P.; Dalvi, S. V.; Mishra, A. Enhancing Aqueous Solubility and Antibacterial Activity of Curcumin by Complexing with Cell-Penetrating Octaarginine. *ACS Omega* **2020**, *5* (30), 19004–19013. https://doi.org/10.1021/acsomega.0c02321.

(38) Dai, C.; Lin, J.; Li, H.; Shen, Z.; Wang, Y.; Velkov, T.; Shen, J. The natural product curcumin as an antibacterial agent: current achievements and problems. *Antioxidants* **2022**, *11* (3), 459. https://doi.org/10.3390/antiox11030459.

(39) Ganvit, V. M.; Bhandari, P. D.; Kunjadiya, A.; Mansuri, J.; Bambhaniya, S. B.; Mandot, A. A.; Sharma, R. K. Waterborne polyurethane polymer dispersions using castor oil and

curcumin as bioresources: synthesis, characterization, and antibacterial textile applications. *Journal of Applied Polymer Science* **2024**, *141* (24), e55509. https://doi.org/10.1002/app.55509.